

1 **Examining Longitudinal Markers of Bladder Cancer Recurrence Through a Semi-**  
2 **Autonomous Machine Learning System for Quantifying Specimen Atypia from Urine**  
3 **Cytology**

4 Joshua J. Levy PhD<sup>1,2,3,4,\*</sup>, Natt Chan MS<sup>4</sup>, Jonathan D. Marotti MD<sup>1,5</sup>, Nathalie J. Rodrigues  
5 MD<sup>1</sup>, A. Aziz O. Ismail MD<sup>1,6</sup>, Darcy A. Kerr MD<sup>1,5</sup>, Edward J. Gutmann MD, AM<sup>1,5</sup>, Ryan E.  
6 Glass MD<sup>7</sup>, Caroline P. Dodge<sup>8</sup>, Arief A. Suriawinata MD<sup>1,5</sup>, Brock Christensen PhD<sup>3,9,10</sup>,  
7 Xiaoying Liu MD<sup>1,5,†</sup>, Louis J. Vaickus MD, PhD<sup>1,5,†</sup>

- 8 1. Emerging Diagnostic and Investigative Technologies, Department of Pathology and  
9 Laboratory Medicine, Dartmouth Hitchcock Medical Center, Lebanon, NH, 03766
- 10 2. Department of Dermatology, Dartmouth Hitchcock Medical Center, Lebanon, NH, 03766
- 11 3. Department of Epidemiology, Dartmouth College Geisel School of Medicine, Hanover,  
12 NH, 03756
- 13 4. Program in Quantitative Biomedical Sciences, Dartmouth College Geisel School of  
14 Medicine, Hanover, NH, 03756
- 15 5. Dartmouth College Geisel School of Medicine, Hanover, NH, 03756
- 16 6. White River Junction VA Medical Center, White River Junction, VT, 05009
- 17 7. UPMC East, Pittsburg, PA, 15146
- 18 8. Cambridge Health Alliance, Cambridge, MA, 02139
- 19 9. Department of Molecular and Systems Biology, Dartmouth College Geisel School of  
20 Medicine, Hanover, NH, 03756
- 21 10. Department of Community and Family Medicine, Dartmouth College Geisel School of  
22 Medicine, Hanover, NH, 03756

23 \* To whom correspondence should be addressed: [joshua.j.levy@dartmouth.edu](mailto:joshua.j.levy@dartmouth.edu)

24 † Authors contributed equally

25  
26 **Author Contributions**

27 JL and LV: conceptualization, formal analysis, funding acquisition, investigation, methodology,  
28 project administration, resources, software, supervision, validation, visualization, writing -  
29 original draft; XL, JM, DK, EG, RG, CD, LV, NR: data curation; all authors: writing - review  
30 and editing

31  
32 **Conflict of Interest**

33 None to disclose.

34  
35 **Funding Sources**

36 JL is supported by NIH subawards P20GM104416 and P20GM130454

37  
38 **Precis**

39 This study used AutoParis-X, a machine learning tool, to extract imaging features from urine  
40 cytology exams to predict recurrence risk in bladder cancer patients. The results demonstrate that  
41 quantitative features of urine specimen atypia can predict recurrence as well or better than  
42 traditional cytological/histological assessments alone and can potentially complement traditional  
43 methods of assessment in screening programs pending further development and validation of  
44 computational methods which leverage multiple longitudinal cytology exams.

45 **Abstract**

46 Urine cytology (UC) is generally considered the primary approach for screening for recurrence  
47 of bladder cancer. However, it is currently unclear how best to use cytological exams themselves  
48 for the assessment and early detection of recurrence, beyond identifying a positive finding which  
49 requires more invasive methods to confirm recurrence and decide on therapeutic options. As  
50 screening programs are frequent, and can be burdensome, finding quantitative means to reduce  
51 this burden for patients, cytopathologists and urologists is an important endeavor and can  
52 improve both the efficiency and reliability of findings. Additionally, identifying ways to risk-  
53 stratify patients is crucial for improving quality of life while reducing the risk of future  
54 recurrence or progression of the cancer. In this study, we leveraged a computational machine  
55 learning tool, AutoParis-X, to extract imaging features from UC exams longitudinally to study  
56 the predictive potential of urine cytology for assessing recurrence risk. This study examined how  
57 the significance of imaging predictors changes over time before and after surgery to determine  
58 which predictors and time periods are most relevant for assessing recurrence risk. Results  
59 indicate that imaging predictors extracted using AutoParis-X can predict recurrence as well or  
60 better than traditional cytological / histological assessments alone and that the predictiveness of  
61 these features is variable across time, with key differences in overall specimen atypia identified  
62 immediately before tumor recurrence. Further research will clarify how computational methods  
63 can be effectively utilized in high volume screening programs to improve recurrence detection  
64 and complement traditional modes of assessment.

65

## 66 **Introduction**

67 Urothelial carcinoma ranks ninth worldwide in cancer incidence as the seventh most common  
68 malignancy in men and seventeenth in women<sup>1-3</sup>. In the United States, urinary bladder cancer  
69 (UBC) is the fourth most common cancer in men and tenth in women. Of urothelial cancer cases,  
70 most are forms of UBC at approximately 90%, while upper tract urothelial carcinomas account  
71 for 5-10% of malignancies<sup>4-7</sup>. The 5-year relative survival rates for UBC patients range from  
72 97% at Stage I to 22% at Stage IV<sup>8-11</sup>. Most UBC incidences (75-85%) are non-muscle invasive  
73 (NMIBC) at first diagnosis, of which 70% register as pTa (noninvasive papillary carcinoma),  
74 20% as pT1, and 10% as carcinoma in situ (CIS) lesions, pTis. The prognosis of NMIBC is  
75 generally favorable, although 30-80% of cases will recur and 1-45% of cases will progress to  
76 muscle invasion within five years<sup>12</sup>. As a result, NMIBC is treated as a chronic disease with a  
77 variety of oncological outcomes that require frequent follow-ups for monitoring and repeated  
78 treatments, giving it the highest cost-per-patient from diagnosis to death of all cancers<sup>13</sup>.

79  
80 The standard approach to patients with symptoms suggestive of UBC involve a combination of  
81 urine cytology, cystoscopy (potentially with tissue biopsy(s)), and immunocytochemical and  
82 molecular studies with longitudinal follow-up for negative and atypical findings<sup>14-23</sup>. After a  
83 positive diagnosis of UBC, urine cytology remains an essential longitudinal monitoring tool for  
84 patients. However, urine cytology suffers from susceptibility to issues such as specimen quality,  
85 inter/intra-observer variability, and ‘hedging’ towards atypical diagnosis, making it a semi-  
86 qualitative assessment and vulnerable to individual biases<sup>24-28</sup>. Such factors restrict the  
87 predictive value of urine cytology therefore increasing reliance on invasive cystoscopy.

88

89 Cytology specimens have historically been tedious to screen, in part due to the sheer volume of  
90 specimens to examine, resulting from regular periodic follow-up and the highly variable  
91 specimen cellularity. While positive and negative urine cytology specimens are easier to classify,  
92 atypical and suspicious urine samples are more challenging and feature poor inter-observer  
93 reproducibility. In recent years, The Paris System for Reporting Urinary Cytology (TPS),  
94 published in 2016 and updated in 2022, has established itself as the widely accepted  
95 classification system for UBC screening <sup>24,29,30</sup>. It devised to tackle the challenges posed by  
96 atypical urines and improve reproducibility <sup>31,32</sup>. Computer algorithms such as the AutoParis  
97 system were designed to ameliorate many of these screening challenges/burdens to make urine  
98 cytology quantitative by employing machine learning techniques that can mimic rapid  
99 examination with TPS criteria <sup>33-39</sup>. AutoParis, and its latest iteration, AutoParis-X, calculate an  
100 Atypia Burden Score (ABS) after cross-tabulating several cellular and cluster-level subjective  
101 and objective indicators of atypia <sup>34,40</sup>.

102  
103 As bladder cancer recurrence is a significant concern for patients and healthcare providers,  
104 various methods have been developed to predict and monitor the likelihood of recurrence. While  
105 computer-aided assessment of the primary tumor has been shown to be predictive of likelihood  
106 for recurrence <sup>41,42</sup>, this examination presents only a snapshot in time, which could be augmented  
107 by repeated urine cytology exams <sup>43-45</sup>. However, there is currently little to no research on how  
108 repeat urine cytology exams can be leveraged to derive longitudinal markers of recurrence <sup>46-49</sup>.

109  
110 Assessing the prognostic capacity of imaging predictors in urine specimens for the treatment of  
111 bladder cancer can have great benefits in reducing clinician workload, improving reproducibility,

112 reducing human error, and lowering treatment cost, in part because cytology predictors can serve  
113 as an “early warning system” for which patients require the most attention/care<sup>50</sup>. In this specific  
114 work, we investigate the potential of using machine learning from urine cytology in predicting  
115 recurrence among a cohort of patients<sup>40</sup>.

116

## 117 **Methods**

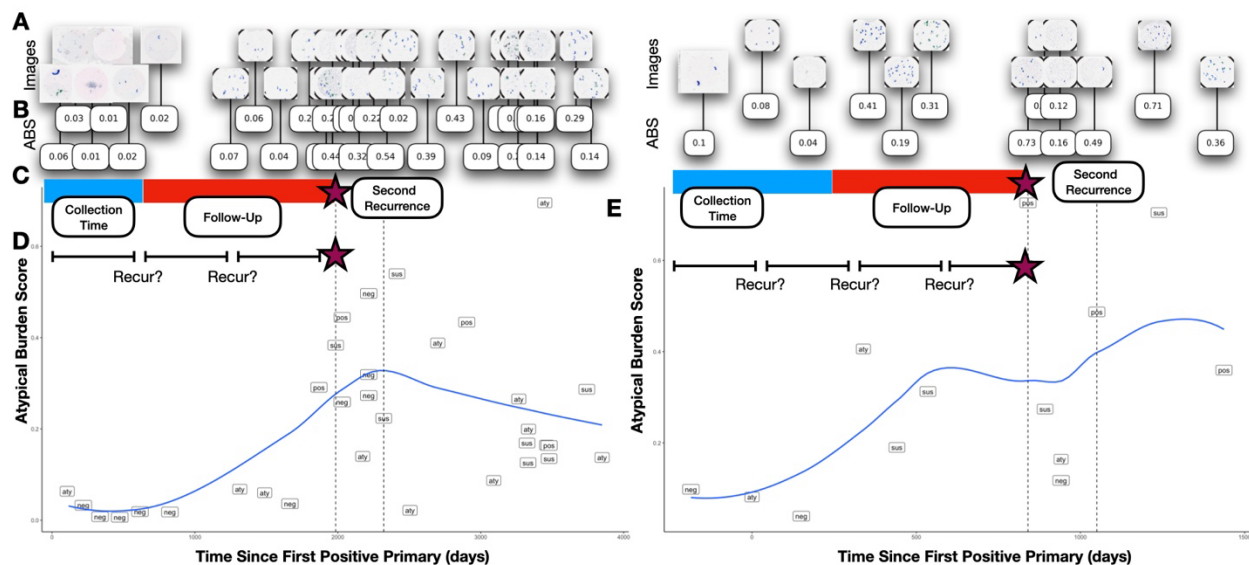
### 118 **Methods Overview**

119 In this section, we summarize the approaches taken to assess the ability to predict time to  
120 recurrence from image-derived UC predictors:

- 121 1. Retrospective review identifies cases with varying follow-up and number of recurrences.
- 122 2. Slide images are scanned (**Figure 1A**) and imaging predictors are extracted from each  
123 whole-slide image (WSI) (**Figure 1B**) using AutoParis-X, which improved upon  
124 techniques introduced by AutoParis<sup>34,40</sup>.
- 125 3. *Fixed predictors* are constructed by aggregating quantitative cytological exam  
126 information across distinct collection periods (i.e., collection time; **Figure 1C**); Cox  
127 proportional hazards models are developed to predict recurrence risk and compare with  
128 manual assessments (UC Class) and tumor grade/stage/type (histology)<sup>51,52</sup>.
- 129 4. *Dynamic predictors* are constructed by utilizing the imaging predictors of each individual  
130 cytology exam; these predictors vary with time (time-varying covariates) and their effects  
131 are reported across different time periods through time-varying coefficient Cox models  
132 (**Figure 1D**)<sup>53,54</sup>.
- 133 5. Models are interpreted by regression coefficients (i.e., hazard ratios), concordance  
134 statistics, and clustering time series, which shows how imaging predictors vary across

135 time for low-risk / high-risk patients with commensurate statistical modeling (e.g.,  
136 hierarchical beta regression) <sup>55,56</sup>.

137



138

139 **Figure 1: Study Overview:** A) UC images are acquired for patients across the study period and  
140 are processed using B) AutoParis-X, which extracts imaging predictors, e.g., ABS; C) Imaging  
141 predictors are aggregated across collection periods to form *fixed predictors* which are then used  
142 to assess time-to-recurrence using Cox models; D) Imaging predictors were also studied  
143 *dynamically* considering results/extracted features from individual tests and their recurrence  
144 potential; risk of recurrence was also studied within specific time periods to demonstrate how the  
145 importance of these predictors varies with time; E) Scatterplots for two patients with time from  
146 the first positive primary versus the Atypia Burden Score as assessed using AutoParis-X; points  
147 were labeled by the UC categories assigned through manual examination of urine cytology

148

## 149 Specimen Collection

150 A total of 1,259 urine specimens collected from 135 bladder cancer patients at Dartmouth-  
151 Hitchcock Medical Center between 2008 and 2019 were retrieved, after institutional review  
152 board approval. The median number of specimens per patient was 8, with an interquartile range  
153 of [8-13] (Figure 1A). Several patients were omitted due to insufficient follow-up or significant  
154 left-censoring which precluded assessment. The specimens were prepared using ThinPrep®

155 (Hologic, Marlborough MA) and Papanicolaou staining before being examined microscopically  
 156 <sup>57</sup>. They were then scanned with a Leica Aperio-AT2 scanner at 40x resolution, resulting in full-  
 157 resolution SVS files (70% quality JPEG compression) representing whole slide images. The  
 158 slides were manually focused on a single plane during scanning, without the use of z-stacking <sup>58</sup>.  
 159 Patient and slide-level characteristics from the retrospective cohort are provided in **Table 1**. All  
 160 slides were evaluated by five cytopathologists to provide diagnoses based on The Paris System  
 161 criteria (negative, atypical, suspicious, positive). Separately, patient characteristics, e.g.,  
 162 hematuria, prior treatments (e.g., BCG– Bacillus Calmette-Guerin or mitomycin) were recorded  
 163 in a secure database <sup>59</sup>. Time to recurrence was determined as indexed from the date of the first  
 164 positive primary tumor as determined through histological examination. Individuals were right  
 165 censored based on last known histological follow-up <sup>60</sup>.

166

167 **Table 1:** Patient and specimen characteristics

Specimens		Patients	
<b>Number Specimens</b>	1259	<b>Number Patients</b>	135
<b>Voided (%)</b>	1110 (88.2)	<b>Age (mean (SD))</b>	71.50 (12.26)
<b>Prior History Hematuria (%)</b>	172 (13.7)	<b>Sex = M (%)</b>	102 (75.6)
<b>Diagnosis (%)</b>		<b>First Positive Primary Tumor Stage/Grade (%)</b>	
<b>Negative</b>	815 (64.7)	<b>0is</b>	7 (5.2)
<b>Atypical</b>	298 (23.7)	<b>T1</b>	35 (25.9)
<b>Suspicious</b>	98 (7.8)	<b>TaLG (non-invasive low grade)</b>	33 (24.4)
<b>Positive</b>	48 (3.8)	<b>TaHG (non-invasive high grade)</b>	60 (44.4)
<b>Contains Artifact (%)</b>	265 (21.0)	<b>Carcinoma in situ (%)</b>	18 (13.3)
		<b>Treatment (%)</b>	
		<b>BCG</b>	71 (52.6)
		<b>Mitomycin</b>	9 (6.7)
		<b>No Treatment</b>	37 (27.4)
		<b>Unavailable</b>	18 (13.3)
		<b>Number of Recurrences (%)</b>	
		<b>0</b>	42 (31.1)

<b>1</b>	73 (54.1)
<b>2</b>	13 (9.6)
<b>3+</b>	7 (5.2)

168

## 169 **Using AutoParis-X to Derive Imaging Predictors of Recurrence**

170 AutoParis-X is a tool for automated assessment of cytology specimens that was developed using  
171 the Python programming language and the PyTorch and Detectron2 frameworks, with statistical  
172 and machine learning models implemented in Python and R <sup>40,61–64</sup>. In brief, this tool:

- 173 1. Utilizes connected components analysis to isolate individual cells and cell clusters
- 174 2. A neural network-based cell border detection model called BorderDet isolates urothelial  
175 cells within clusters and identifies dense overlapping cell architectures <sup>65</sup>.
- 176 3. Additional morphometric measures are derived for cell-type classification and atypia  
177 estimation <sup>34,40</sup>.
- 178 4. A convolutional neural network called UroNet filters out any objects which are not  
179 urothelial cells <sup>34,40</sup>.
- 180 5. A segmentation neural network method called UroSeg estimates the nuclear-to-cytoplasm  
181 ratio <sup>34,40</sup>.
- 182 6. A convolutional neural network called AtyNet scores cells for subjective markers of  
183 atypia <sup>40</sup>.
- 184 7. A machine learning classifier estimates the Atypia Burden Score (ABS) which integrates  
185 cell and cluster-level scores and other demographic and specimen characteristics into a  
186 summary measure of overall specimen atypia <sup>66–68</sup>.
- 187 8. In addition, hierarchical regression models identified important indicators of atypia, and  
188 graphical displays were generated through an interactive web application utilized by our  
189 team of cytopathologists <sup>69,70</sup>.



190 A description of slide level measures and ABS scores, listed in **Supplementary Table 1**, which  
191 were derived for each specimen in this cohort.

192

### 193 **Recurrence Prediction**

194 Time to recurrence was predicted using both traditional cytological measures and AutoParis-X  
195 derived imaging features (**Figure 1B**), controlling for age and sex, prior treatment, tumor grade,  
196 medical history, etc., where possible— e.g., treatment information was largely excluded from  
197 multivariable modeling due to missingness and uncertainty in treatment time.

198

199 *Fixed recurrence predictors.* First, we aggregated imaging/cytology statistics (e.g., average  
200 number of atypical cells) for cytology exams before/at the primary diagnosis date or within a  
201 specific time frame after the primary diagnosis date (i.e., *collection time*) (**Figure 1C**). It is  
202 important to ensure that data is collected up to a specific date in order to accurately assess risk  
203 for new patients. This is because collecting data beyond this point would introduce information  
204 about the future and potentially bias the results. To ensure that the findings remain applicable,  
205 data for new patients must be collected only up to the defined collection time. Cases were  
206 excluded if events/censoring occurred before this collection window and recurrence times were  
207 adjusted as appropriate (i.e., delayed entry) to avoid endogeneity. We denote predictors during  
208 this time period as *fixed predictors*. Fixed predictors were modeled using multivariable cox  
209 proportional hazards models <sup>71</sup>:

$$\begin{aligned} 210 \quad & \text{days\_to\_event}_i | \text{censored}_i = 0 \sim \text{Exponential}(\lambda_i) \\ 211 \quad & \text{days\_to\_event}_i | \text{censored}_i = 0 \sim \text{Exponential} - \text{CCDF}(\lambda_i) \\ 212 \quad & f(y) = \lambda_i e^{-\lambda_i y} \\ 213 \quad & \lambda_i = 1/\mu_i \\ 214 \quad & \log(\mu_i) = x_i^T \beta \\ 215 \end{aligned}$$

216 The predictive performance of leveraging fixed (i.e., collected) UC imaging predictors was  
217 compared to the histological examination, e.g., tumor grade/stage and whether the tumor was  
218 carcinoma in situ (Cis). Separate cox models were fit to the imaging predictors alone, tumor  
219 grade and carcinoma in situ, and both, adjusting for age and sex. Models were compared through  
220 partial likelihood ratio testing, which would indicate whether imaging predictors alone were  
221 more informative than the histological findings (**H<sub>1</sub>: Imaging>Grade+Cis**) and separately  
222 whether the imaging predictors supplemented tumor grade information to add additional  
223 predictive capacity (**H<sub>1</sub>: Imaging+Grade+Cis>Grade+Cis**). We separately reported the hazard  
224 ratios for the imaging predictors after adjusting for tumor grade/stage and Cis. Results were  
225 compared at all collection times. We did not adjust models for whether the patients had  
226 chemotherapy due to unreliability in recording patient start date and adherence, though this  
227 information was recorded in the demographic tables for additional context.

228  
229 *Dynamic recurrence predictors.* Time-dependent predictors (denoted as *dynamic predictors*)  
230 were modeled using cox proportional hazards models which allowed repeat measures by patient.  
231 These predictors were modeled with and without time varying effects (similar to estimating  
232 multiple survival curves across discrete time intervals) (**Figure 1D**), which reports changes to the  
233 relationship between predictors and recurrence as a function of time (i.e., certain intervals may  
234 be more predictive of recurrence) <sup>53</sup>.

235  
236 Individual predictors were modeled in a univariable setting, adjusting only for age and gender.  
237 These variables were combined into multivariable models. Predictor selection was accomplished  
238 using the variance inflation factor (VIF) after fitting the survival models and iteratively removing

239 predictors until the largest VIF score was less than 6.5<sup>72</sup>. We had also performed LASSO  
240 predictor selection but opted for VIF as these models outperformed LASSO<sup>73</sup>. Concordance  
241 statistics (C-index; as reported using the *survival* R package) were reported for the univariable  
242 and multivariable models, along with hazards ratios, confidence intervals and p-values. For the  
243 time-varying effects, hazards ratios and their statistical significance were reported across time for  
244 individual predictors and overall across many predictors<sup>54</sup>. Hazard predictions were  
245 dichotomized into low and high risk and *fixed predictors* were visualized using Kaplan Meier  
246 plots using the *survminer* package (R v4.1)<sup>74</sup>.

247

## 248 **Studying Trajectories of ABS Scores**

249 After fitting the cox models, we additionally sought to uncover longitudinal patterns of atypia  
250 related to high recurrence risk (**Figure 1E**). This was accomplished by clustering the trajectories  
251 of ABS scores across time using dynamic time warping (DTW). DTW was used to construct a  
252 distance matrix between individual patient trajectories, which were reduced into two features per  
253 patient using multi-dimensional scaling using the *scikit-time* library (Python v3.8) and *reticulate*  
254 package (R v4.1)<sup>75,76</sup>. Separately, the patients were clustered using hierarchical clustering of the  
255 DTW distance matrix via the *hclust* function (R v4.1). Cases were omitted if they did not contain  
256 at least two points. Associations between the DTW clusters and features were identified through  
257 generalized linear mixed effects modeling. The average ABS score was visualized across time,  
258 aggregated for low-risk / high-risk patients and separately for the derived clusters at binned time  
259 periods. Beta hierarchical regression models with post-hoc comparison via emmeans were used  
260 to report how ABS differed between high and low risk patients across time<sup>55,56,77</sup>:

$$\begin{aligned} 261 \quad & ABS_i \sim \text{Beta}(\mu_i * \phi_i, (1 - \mu_i) * \phi_i) \\ 262 \quad & g(\mu_i) = \beta_0 + \beta_1 time_i + \beta_2 risk_i + \beta_3 time_i * risk_i + \theta_{patient[i]}; g(\cdot) : (0,1) \rightarrow \mathbb{R} \\ 263 \quad & \theta_{patient[i]} \sim N(0, \tau^2) \end{aligned}$$

264 We identified several patients who had multiple recurrences. We visualized changes in ABS  
265 before and after recurrences by creating scatter plots of ABS versus time. We fit a hierarchical  
266 beta regression model to depict overall changes in ABS score across time between patients' first  
267 and second recurrences, with similar hierarchical beta regression models fit, excluding *risk* from  
268 the model.

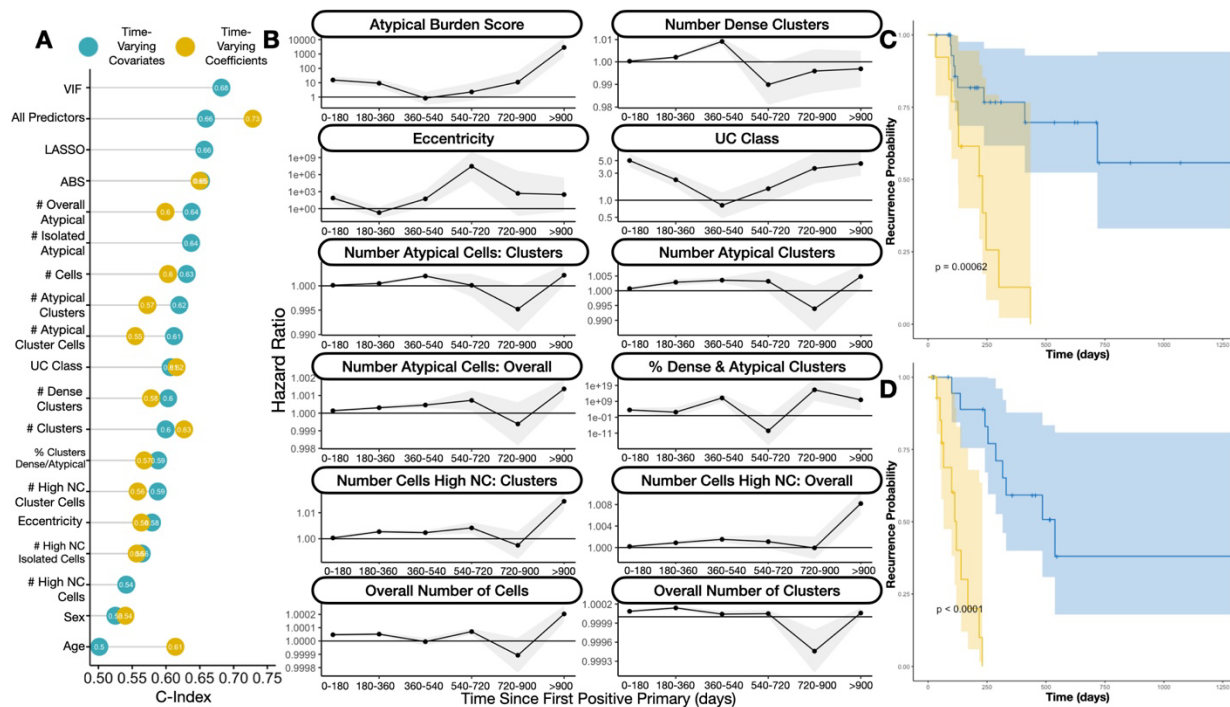
269

## 270 Results

### 271 Recurrence Predicted from Fixed Predictors

272 Fitting cox proportional hazards models at various collection times, we found there was  
273 moderate ability to predict recurrence using UC imaging predictors (**Figure 2C,D;**  
274 **Supplementary Figure 1; Supplementary Table 2**). When only collecting cytological  
275 information up to the first positive primary (collection time = 0 days), imaging and manually  
276 assessed UC class predictors yielded a C-index of 0.672. Overall, imaging predictors were more  
277 informative than manual cytological examination (**Supplementary Table 2**, see “% Outperform  
278 UC Class”, number of imaging predictor with better performance than manual examination). The  
279 predictiveness of the UC imaging predictors increased when predictors were aggregated across  
280 larger time intervals / collection times, for instance yielding a C-index of 0.77 when collecting  
281 quantitative cytological information over the first 180 days after the first positive primary  
282 (collection time = 180 days). Collecting cytological information past this point in time and  
283 aggregating yielded marginal to no additional information on recurrence. The imaging variables

284 differed significantly in their predictive capacity. Surprisingly, imaging features extracted from  
 285 urothelial cell clusters proved remarkably predictive (C-index for: number of atypical cell  
 286 clusters = 0.733; number of dense cell clusters = 0.748 at collection time 180 days) as opposed to  
 287 variables which correlate more closely with UC Class (e.g., ABS).  
 288  
 289 Imaging predictors extracted from cytology and separately in conjunction with risk assessment  
 290 models based on tumor grade/type were more informative for recurrence risk prediction than that  
 291 derived from tumor grade/type alone (**Supplementary Figure 2; Supplementary Table 3**), as  
 292 assessed through partial likelihood ratio testing<sup>78,79</sup>. At nearly every collection interval, imaging  
 293 predictors demonstrated statistically significantly better predictive capacity than tumor  
 294 grade/type alone and effects from the imaging predictors were highly statistically significant,  
 295 even after adjusting for tumor grade/type (**Supplementary Table 3**).  
 296



297

298 **Figure 2: Findings from Recurrence Risk Models:** A) Dot chart indicating concordance  
299 statistics for each of the imaging predictors for the *time-varying covariate* and *time-varying*  
300 *effects* cox proportional hazards models; UC class stands for category assigned via manual  
301 examination by the cytopathologist; VIF and LASSO refer to multivariable models with the  
302 respective predictor selection methods; All/Overall predictors refers to multivariable models with  
303 all imaging predictors; B) Ribbon plot illustrating hazard ratios and confidence intervals for  
304 univariable *time-varying effects* cox proportional hazards model for individual imaging  
305 predictors, demonstrating differing associations with recurrence at distinct time intervals; C)  
306 Kaplan-Meier plot and rank-based statistic for *fixed imaging predictors* collected before or up to  
307 the date of the first positive primary, reported for low (blue) and high (yellow) risk patients as  
308 assessed using the Cox model; D) similar KM plot for patients with 90 days of follow-up  
309 information collected, predicting recurrence risk after this collection period

310

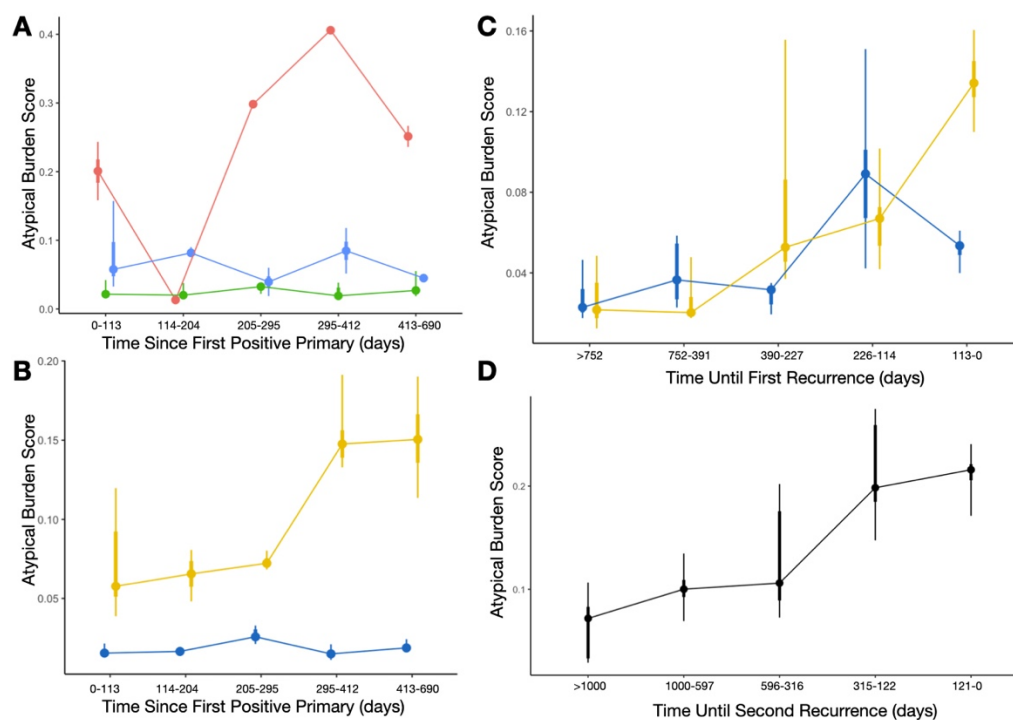
### 311 **Recurrence Predicted from Dynamic Predictors**

312 When considering all individual cytology exams dynamically over time (*time-varying*  
313 *covariates*) and not aggregating across distinct time windows, imaging predictors corresponded  
314 with recurrence with a C-index of 0.66 (**Figure 2A; Supplementary Table 2**). The Atypical  
315 Score (C-index=0.65) was more predictive than UC Class (C-index=0.58) using this approach.  
316 Fitting recurrence models, allowing effects of different predictors to vary— these time varying  
317 effects were reported for each distinct time period (*time-varying effects*; association between  
318 variables and recurrence risk updated every half year; **Figure 2B**), achieved an overall C-index  
319 of 0.73, greater than that offered by the *time-varying covariates*. The Atypical Score (C-  
320 index=0.65) was still more predictive than UC Class (C-index=0.62) using this approach  
321 (**Supplementary Table 4**). The association between individual imaging predictors and  
322 recurrence risk varied across these intervals (**Figure 2B; Supplementary Table 5**). For instance,  
323 ABS and UC Class were highly positively associated with recurrence risk during the first year  
324 and after the second year of follow-up (**Figure 2B; Supplementary Table 5**). As another  
325 example, the number of atypical cells and atypical clusters demonstrated their greatest

326 association with recurrence risk at intermediate intervals (e.g., 180-540 days) (**Figure 2B**;  
327 **Supplementary Table 5**).

328

### 329 Trajectory Cluster Analysis



330

331 **Figure 3: Atypia Burden Scores reported across time, aggregated across distinct time**  
332 **periods using point interval plots: A)** Each curve/color represents ABS scores from patients  
333 belonging to three different temporal trajectories (red, blue, green clusters), determined using the  
334 time series clustering and summarized using the aggregate statistics for each time period; **B)**  
335 Each curve is colored based on low (blue) and high (yellow) risk patients, measured from the  
336 time since first positive primary; **C)** Comparing ABS scores between low/high risk patients,  
337 similar to the previous plot, with cytological exams grouped by days until the first recurrence  
338 instead of from the date of the first positive primary; **D)** ABS scores, combined across distinct  
339 time periods, for patients from the first until the second recurrence, grouped by the days until the  
340 second recurrence, demonstrating increasing atypia prior to the recurrence finding

341

342 We sought to study the trajectories of specimen atypia from the first positive primary to the first  
343 recurrence. Time series clustering yielded three independent clusters (**Figure 3A**). The red

344 cluster (**Figure 3A**) revealed the tendency of patients to exhibit a decrease in specimen atypia  
345 immediately after the positive primary (likely resulting from previous treatment), followed by a  
346 sharp increase in specimen atypia thereafter. Patients deemed high risk by the Cox models  
347 (**Figure 3B,C**) initially have a low atypical burden, similar to the low risk group. However, over  
348 time after the positive primary, the discrepancies in specimen atypia increase substantially  
349 (**Figure 3B; Supplementary Table 6**). When counting down backwards from the date of first  
350 recurrence, we see that specimen atypia increases steadily from both low and high risk patients  
351 prior to the first recurrence. Within 3-4 months prior to the first recurrence, specimen atypia for  
352 the low-risk patients decreases while continuing to increase for the high risk patients (**Figure**  
353 **3C; Supplementary Table 6**).

354  
355 These trends were similarly identified for patients who had a first recurrence who would go onto  
356 have a second recurrence (**Figure 3D; Supplementary Table 6; Supplementary Figure 3**). A  
357 statistically significant increase in overall specimen atypia over time was identified during this  
358 interval between the first and second recurrences (**Supplementary Table 6**). The Atypia Burden  
359 Scores plotted across time from positive primary date for patients with multiple recurrences can  
360 be found in **Supplementary Figure 4**, though an in-depth assessment is outside of the scope of  
361 this study.

## 362 363 **Discussion**

364 Bladder cancer has a high rate of recurrence, which requires frequent follow up screening and  
365 monitoring. By using advanced computer algorithms, it is possible to create a non-invasive,  
366 semi-autonomous system that can analyze repeat cytology exams and provide highly precise



367 markers of specimen atypia<sup>34,36,40</sup>. This approach can improve our understanding of how bladder  
368 cancer progresses and recurs, as well as identify patterns that indicate early detection of  
369 recurrence. This study sought to investigate the potential utility of such an approach, made  
370 possible by the AutoParis-X tool, which can facilitate rapid examination of cytology specimens  
371<sup>40</sup>. Imaging predictors derived using AutoParis-X such as the Atypia Burden Score and other  
372 sub-scores (e.g., number of atypical clusters) were followed across time for patients and were  
373 aggregated across distinct time periods and studied *dynamically* to predict bladder cancer  
374 recurrence.

375  
376 The principal findings from our study are twofold: 1) urine cytology exam results can inform  
377 recurrence risk, and imaging predictors extracted through the use of machine learning can be  
378 more informative of recurrence than manual cytological and/or histological examination alone;  
379 and 2) the predictive value of imaging predictors extracted from UC exams varies across time  
380 (both in terms of combining information from previous exams and real-time predictiveness of  
381 time-variant predictors). Our findings support and add to previous studies showing that  
382 preoperative urine cytology examination can predict recurrence<sup>80-82</sup>. We also found that  
383 collecting and combining cytological information with summary statistics within the first six  
384 months after the positive primary diagnosis is important for assessing recurrence risk for patients  
385 who have not yet recurred. While there are several other machine learning techniques which  
386 have been developed to perform histological assessments of recurrence risk from the primary site  
387 at the time of resection, cytological assessments are far less invasive (requiring the patient to  
388 simply void into a collection cup in most cases)<sup>41,83</sup>. Due to routine screening via UC, more  
389 information is available, which when assessed in totality, can be highly predictive of recurrence.

390 It is important to consider how information from cytological and histological examinations can  
391 be used together to provide more comprehensive assessment of risk. The use of imaging  
392 predictors extracted from cytology, both alone and in combination with tumor grade/type,  
393 provided more useful information for predicting recurrence risk compared to relying on tumor  
394 grade/type alone, as determined through partial likelihood ratio testing. The combination of  
395 cytological and histological assessments is especially pertinent for patients who have undergone  
396 a tumor resection and are identified to be at high risk from both cytology and histology.

397  
398 There are limitations to this study. For instance, there is still ample room to improve the  
399 AutoParis-X algorithm, which can impact the reliability of these predictors<sup>40</sup>. Furthermore, we  
400 have not studied its utility in augmenting medical diagnostic decision-making in conjunction  
401 with the cytopathologist<sup>84-88</sup>. Changes in specimen preparation across the past decade and a half  
402 may have impacted imaging predictors estimated using AutoParis-X. We used the last  
403 histological follow up exam with a negative finding as a right censoring event for patients in this  
404 cohort who did not ultimately develop recurrence<sup>89</sup>. As this was a retrospective cohort study  
405 with sporadic follow-up (typically every three months as specified by guidelines), it was  
406 challenging to identify suitable follow-up and censorship criteria. Furthermore, death may  
407 present a competing risk to recurrence, which could potentially bias effect estimates. While  
408 methods do exist to account for competing risks, relevant statistical methods and their  
409 computational implementations are underdeveloped and inaccessible in the context of time-  
410 varying covariates and effects<sup>90,91</sup>. These limitations will be improved upon in further  
411 assessments of this tool and these study findings should be interpreted in the context of an  
412 exploratory analysis. The study cohort was restricted to individuals from Northern New England

413 and findings are applicable to this population— expansion of this study to large, diverse study  
414 cohorts from geographically disparate regions will improve the generalizability of these findings.

415  
416 In the future, we plan to leverage additional machine learning techniques which are suitable for  
417 recurrence prediction. For instance, tree-boosting approaches and deep learning models exist  
418 which are well-suited for the study of longitudinal / time-to-event data <sup>92–105</sup>. They can reveal  
419 interactions between predictors for use in statistical modeling as well as identify cytology exams  
420 / timepoints which are most informative of recurrence <sup>106</sup>. These are estimated dynamically using  
421 sophisticated computational heuristics and are an area of future follow-up.

422  
423 The results of this study highlight the need for further research comparing the performance of the  
424 AutoParis-X system with other non-invasive methods for assessing the potential for bladder  
425 cancer recurrence. Many promising approaches make use of various molecular assays developed  
426 for liquid biopsies, and several screening programs have also been developed that use a  
427 combination of different assays to assess the potential for recurrence <sup>107–114</sup>. These should be  
428 considered for comparison when attempting to roll out potential screening systems/guidelines.  
429 While early detection of recurrence is important, it is currently unclear what the next steps  
430 should be in terms of treatment and management given the adoption of computational systems  
431 for real-time recurrence assessment <sup>35,39,115–117</sup>. This is an area that requires further research.  
432 Furthermore, there are a wide-range of epidemiological studies which could benefit from  
433 incorporating cytological information. For instance, exposure to high levels of arsenic in  
434 drinking water and cigarette smoking are associated with bladder cancer risk and could benefit

435 from being studied in conjunction with advanced computational methods for urine cytology <sup>118-</sup>  
436 <sup>123</sup>.

437

#### 438 **Conclusion**

439 This study sought to investigate the potential benefit of using computer algorithms to extract  
440 highly quantitative, longitudinal cytological features can be used to inform the risk of recurrence  
441 for bladder cancer patients. We found that image predictors extracted using the AutoParis-X  
442 system were indeed associated with tumor recurrence, in many cases more so than traditional  
443 modes of cytological/histological examination, and that the importance/predictiveness of these  
444 predictors varied across time from the positive primary. While this study demonstrates the  
445 potential utility for computerized systems to supplement and make use of screening programs  
446 with a large number of follow up visits, further research is warranted to better understand how  
447 these systems can be integrated into such screening programs.

448

449 **References**

- 450
- 451 1. Kaufman, D. S., Shipley, W. U. & Feldman, A. S. Bladder cancer. *The Lancet* **374**,
- 452 239–249 (2009).
- 453 2. Sanli, O. *et al.* Bladder cancer. *Nature reviews Disease primers* **3**, 1–19 (2017).
- 454 3. Shalata, A. T. *et al.* Predicting Recurrence of Non-Muscle-Invasive Bladder Cancer:
- 455 Current Techniques and Future Trends. *Cancers* **14**, 5019 (2022).
- 456 4. van der Meijden, A. *et al.* Significance of bladder biopsies in Ta, T1 bladder tumors:
- 457 a report from the EORTC Genito-Urinary Tract Cancer Cooperative Group.
- 458 *European urology* **35**, 267–271 (1999).
- 459 5. Lokeshwar, V. B. & Soloway, M. S. Current bladder tumor tests: does their
- 460 projected utility fulfill clinical necessity? *The Journal of urology* **165**, 1067–1077
- 461 (2001).
- 462 6. Griffiths, T. L. & Cancer, A. on B. Current perspectives in bladder cancer
- 463 management. *International journal of clinical practice* **67**, 435–448 (2013).
- 464 7. DeGeorge, K. C., Holt, H. R. & Hodges, S. C. Bladder cancer: diagnosis and
- 465 treatment. *American family physician* **96**, 507–514 (2017).
- 466 8. *AJCC Cancer Staging Manual*. (Springer International Publishing, 2017).
- 467 9. Rabbani, F., Perrotti, M., Russo, P. & Herr, H. W. Upper-tract tumors after an initial
- 468 diagnosis of bladder cancer: argument for long-term surveillance. *J Clin Oncol* **19**,
- 469 94–100 (2001).
- 470 10. Zang, Y., Li, X., Cheng, Y., Qi, F. & Yang, N. An overview of patients with
- 471 urothelial bladder cancer over the past two decades: a Surveillance, Epidemiology,
- 472 and End Results (SEER) study. *Ann Transl Med* **8**, 1587 (2020).
- 473 11. Schroeck, F. R. *et al.* Determinants of Risk-Aligned Bladder Cancer Surveillance—
- 474 Mixed-Methods Evaluation Using the Tailored Implementation for Chronic
- 475 Diseases Framework. *JCO Oncology Practice* **18**, e152–e162 (2022).
- 476 12. van Rhijn, B. W. G. *et al.* Recurrence and Progression of Disease in Non–Muscle-
- 477 Invasive Bladder Cancer: From Epidemiology to Treatment Strategy. *European*
- 478 *Urology* **56**, 430–442 (2009).
- 479 13. Mossanen, M. & Gore, J. L. The burden of bladder cancer care: direct and indirect
- 480 costs. *Curr Opin Urol* **24**, 487–491 (2014).
- 481 14. Bostwick, D. G. 7 - Urine Cytology. in *Urologic Surgical Pathology (Fourth Edition)*
- 482 (eds. Cheng, L., MacLennan, G. T. & Bostwick, D. G.) 322-357.e7 (Elsevier, 2020).
- 483 15. Stenzl, A., Hennenlotter, J. & Schilling, D. Can we still afford bladder cancer?
- 484 *Current Opinion in Urology* **18**, 488 (2008).
- 485 16. Bruins, H. M. *et al.* The Importance of Hospital and Surgeon Volume as Major
- 486 Determinants of Morbidity and Mortality After Radical Cystectomy for Bladder
- 487 Cancer: A Systematic Review and Recommendations by the European Association
- 488 of Urology Muscle-invasive and Metastatic Bladder Cancer Guideline Panel.
- 489 *European Urology Oncology* **3**, 131–144 (2020).
- 490 17. Parekattil, S. J., Fisher, H. A. & Kogan, B. A. Neural network using combined urine
- 491 nuclear matrix protein-22, monocyte chemoattractant protein-1 and urinary
- 492 intercellular adhesion molecule-1 to detect bladder cancer. *The Journal of urology*
- 493 **169**, 917–920 (2003).
- 494 18. Halling, K. C. *et al.* A comparison of BTA stat, hemoglobin dipstick, telomerase and
- 495 Vysis UroVysion assays for the detection of urothelial carcinoma in urine. *The*
- 496 *Journal of urology* **167**, 2001–2006 (2002).

- 497 19. Todenhöfer, T. *et al.* Stepwise application of urine markers to detect tumor  
498 recurrence in patients undergoing surveillance for non-muscle-invasive bladder  
499 cancer. *Disease markers* **2014**, (2014).
- 500 20. Hendricksen, K. *et al.* Discrepancy Between European Association of Urology  
501 Guidelines and Daily Practice in the Management of Non-muscle-invasive Bladder  
502 Cancer: Results of a European Survey. *European Urology Focus* **5**, 681–688 (2019).
- 503 21. Raab, S. S., Grzybicki, D. M., Vrbin, C. M. & Geisinger, K. R. Urine cytology  
504 discrepancies: frequency, causes, and outcomes. *Am J Clin Pathol* **127**, 946–953  
505 (2007).
- 506 22. Zuiverloon, T. C. M., de Jong, F. C. & Theodorescu, D. Clinical Decision Making in  
507 Surveillance of Non-Muscle-Invasive Bladder Cancer: The Evolving Roles of  
508 Urinary Cytology and Molecular Markers. *Oncology (Williston Park)* **31**, 855–862  
509 (2017).
- 510 23. Lin, D. W., Herr, H. W. & Dalbagni, G. Value of urethral wash cytology in the  
511 retained male urethra after radical cystoprostatectomy. *J Urol* **169**, 961–963 (2003).
- 512 24. Levy, J. J. *et al.* Large-scale longitudinal comparison of urine cytological  
513 classification systems reveals potential early adoption of The Paris System criteria.  
514 *J Am Soc Cytopathol* S2213-2945(22)00241-1 (2022) doi:10.1016/j.jasc.2022.08.001.
- 515 25. Celik, B. & Kavas, G. Atypical category of the Johns Hopkins Template has higher  
516 ROM than the Paris System but the Paris system is more applicable for suspicious  
517 category. *Acta Cytol* (2023) doi:10.1159/000529484.
- 518 26. Morency, E. & Antic, T. Atypical urine cytology and the Johns Hopkins Hospital  
519 template: the University of Chicago experience. *J Am Soc Cytopathol* **3**, 295–302  
520 (2014).
- 521 27. Rai, S. *et al.* A Quest for Accuracy: Evaluation of The Paris System in Diagnosis of  
522 Urothelial Carcinomas. *J Cytol* **36**, 169–173 (2019).
- 523 28. Tian, W., Shore, K. T. & Shah, R. B. Significant reduction of indeterminate (atypical)  
524 diagnosis after implementation of The Paris System for Reporting Urinary  
525 Cytology: A single-institution study of more than 27,000 cases. *Cancer Cytopathology*  
526 **129**, 114–120 (2021).
- 527 29. Barkan, G. A. *et al.* The Paris System for Reporting Urinary Cytology: The Quest to  
528 Develop a Standardized Terminology. *ACY* **60**, 185–197 (2016).
- 529 30. Wojcik, E. M., Kurtycz, D. F. & Rosenthal, D. L. *The Paris system for reporting urinary*  
530 *cytology*. (Springer, 2022).
- 531 31. Kurtycz, D. F. *et al.* Paris interobserver reproducibility study (PIRST). *Journal of the*  
532 *American Society of Cytopathology* **7**, 174–184 (2018).
- 533 32. Long, T. *et al.* Interobserver reproducibility of The Paris System for Reporting  
534 Urinary Cytology. *Cytojournal* **14**, 17 (2017).
- 535 33. Lebret, T. *et al.* VISIOCYT1 clinical trial: Artificial intelligence for the diagnosis of  
536 bladder urothelial lesions. *JCO* **40**, e16558–e16558 (2022).
- 537 34. Vaickus, L. J., Suriawinata, A. A., Wei, J. W. & Liu, X. Automating the Paris System  
538 for urine cytopathology—A hybrid deep-learning and morphometric approach.  
539 *Cancer Cytopathology* **127**, 98–115 (2019).
- 540 35. McAlpine, E. D., Pantanowitz, L. & Michelow, P. M. Challenges Developing Deep  
541 Learning Algorithms in Cytology. *ACY* **65**, 301–309 (2021).
- 542 36. Sanghvi, A. B., Allen, E. Z., Callenberg, K. M. & Pantanowitz, L. Performance of an  
543 artificial intelligence algorithm for reporting urine cytopathology. *Cancer*  
544 *Cytopathology* **127**, 658–666 (2019).

- 545 37. Awan, R. *et al.* Deep learning based digital cell profiles for risk stratification of  
546 urine cytology images. *Cytometry Part A* **99**, 732–742 (2021).
- 547 38. Kaneko, M. *et al.* Urine cell image recognition using a deep-learning model for an  
548 automated slide evaluation system. *BJU Int* (2021) doi:10.1111/bju.15518.
- 549 39. Landau, M. S. & Pantanowitz, L. Artificial intelligence in cytopathology: a review  
550 of the literature and overview of commercial landscape. *J Am Soc Cytopathol* **8**, 230–  
551 241 (2019).
- 552 40. Levy, J. *et al.* Large-Scale Validation Study of an Improved Semi-Autonomous  
553 Urine Cytology Assessment Tool: AutoParis-X. 2023.03.01.23286639 Preprint at  
554 <https://doi.org/10.1101/2023.03.01.23286639> (2023).
- 555 41. Barrios, W. *et al.* Bladder cancer prognosis using deep neural networks and  
556 histopathology images. *Journal of Pathology Informatics* **13**, 100135 (2022).
- 557 42. Lucas, M. *et al.* Deep Learning–based Recurrence Prediction in Patients with Non-  
558 muscle-invasive Bladder Cancer. *European Urology Focus* **8**, 165–172 (2022).
- 559 43. Karakiewicz, P. I. *et al.* Institutional variability in the accuracy of urinary cytology  
560 for predicting recurrence of transitional cell carcinoma of the bladder. *BJU Int* **97**,  
561 997–1001 (2006).
- 562 44. Lotan, Y. *et al.* Clinical comparison of noninvasive urine tests for ruling out  
563 recurrent urothelial carcinoma. *Urologic Oncology: Seminars and Original*  
564 *Investigations* **35**, 531.e15-531.e22 (2017).
- 565 45. Schroeck, F. R. *et al.* Data-driven approach to implementation mapping for the  
566 selection of implementation strategies: a case example for risk-aligned bladder  
567 cancer surveillance. *Implementation Sci* **17**, 58 (2022).
- 568 46. Sullivan, P. S., Chan, J. B., Levin, M. R. & Rao, J. Urine cytology and adjunct  
569 markers for detection and surveillance of bladder cancer. *Am J Transl Res* **2**, 412–440  
570 (2010).
- 571 47. Nabi, G., Greene, D. R. & O'Donnell, M. How Important is Urinary Cytology in the  
572 Diagnosis of Urological Malignancies? *European Urology* **43**, 632–636 (2003).
- 573 48. Kent, D. L., Nease, R. A., Sox, H. C., Shortliffe, L. D. & Shachter, R. Evaluation of  
574 Nonlinear Optimization for Scheduling of follow-up cystoscopies to Detect  
575 Recurrent Bladder Cancer. *Med Decis Making* **11**, 240–248 (1991).
- 576 49. Schrag, D. *et al.* Adherence to Surveillance Among Patients With Superficial  
577 Bladder Cancer. *JNCI: Journal of the National Cancer Institute* **95**, 588–597 (2003).
- 578 50. van, der A. M. N. M. *et al.* Cystoscopy Revisited as the Gold Standard for  
579 Detecting Bladder Cancer Recurrence: Diagnostic Review Bias in the Randomized,  
580 Prospective CEFUB Trial. *Journal of Urology* **183**, 76–80 (2010).
- 581 51. Schober, P. & Vetter, T. R. Survival Analysis and Interpretation of Time-to-Event  
582 Data: The Tortoise and the Hare. *Anesth Analg* **127**, 792–798 (2018).
- 583 52. Lin, D. Y. & Wei, L. J. The Robust Inference for the Cox Proportional Hazards  
584 Model. *Journal of the American Statistical Association* **84**, 1074–1078 (1989).
- 585 53. Fisher, L. D. & Lin, D. Y. Time-Dependent Covariates in the Cox Proportional-  
586 Hazards Regression Model. *Annual Review of Public Health* **20**, 145–157 (1999).
- 587 54. Scheike, T. H. Time-Varying Effects in Survival Analysis. in *Handbook of Statistics*  
588 vol. 23 61–85 (Elsevier, 2003).
- 589 55. Cribari-Neto, F. & Zeileis, A. Beta Regression in R. *Journal of Statistical Software* **34**,  
590 1–24 (2010).
- 591 56. Brooks, M. E. *et al.* glmmTMB balances speed and flexibility among packages for  
592 Zero-inflated Generalized Linear Mixed Modeling. *R Journal* **9**, 378–400 (2017).

- 593 57. Okuda, C. *et al.* Quantitative cytomorphological comparison of SurePath and  
594 ThinPrep liquid-based cytology using high-grade urothelial carcinoma cells.  
595 *Cytopathology* **32**, 654–659 (2021).
- 596 58. Kim, D. *et al.* Evaluating the role of Z-stack to improve the morphologic evaluation  
597 of urine cytology whole slide images for high-grade urothelial carcinoma: Results  
598 and review of a pilot study. *Cancer Cytopathology* **130**, 630–639 (2022).
- 599 59. B, Ö. A., Jocham, D. & Bock, P. R. Intravesical Bacillus Calmette-Guerin Versus  
600 Mitomycin C For Superficial Bladder Cancer: A Formal Meta-Analysis of  
601 Comparative Studies on Recurrence and Toxicity. *Journal of Urology* **169**, 90–95  
602 (2003).
- 603 60. Chen, H. *et al.* Urine cytology in monitoring recurrence in urothelial carcinoma  
604 after radical cystectomy and urinary diversion. *Cancer Cytopathology* **124**, 273–278  
605 (2016).
- 606 61. Tippmann, S. Programming tools: Adventures with R. *Nature* **517**, 109–110 (2015).
- 607 62. Matthes, E. *Python Crash Course, 2nd Edition: A Hands-On, Project-Based Introduction*  
608 *to Programming*. (No Starch Press, 2019).
- 609 63. Paszke, A. *et al.* PyTorch: An Imperative Style, High-Performance Deep Learning  
610 Library. *arXiv:1912.01703 [cs, stat]* (2019).
- 611 64. Wu, Y., Kirillov, A., Massa, F., Lo, W.-Y. & Girshick, R. Detectron2. (2019).
- 612 65. Levy, J. J. *et al.* Uncovering additional predictors of urothelial carcinoma from  
613 voided urothelial cell clusters through a deep learning-based image preprocessing  
614 technique. *Cancer Cytopathol* (2022) doi:10.1002/cncy.22633.
- 615 66. Sigrist, F. Latent Gaussian Model Boosting. *IEEE Transactions on Pattern Analysis*  
616 *and Machine Intelligence* 1–1 (2022) doi:10.1109/TPAMI.2022.3168152.
- 617 67. Sigrist, F. Gaussian Process Boosting. *Journal of Machine Learning Research* **23**, 1–46  
618 (2022).
- 619 68. Tan, Y. V. & Roy, J. Bayesian additive regression trees and the General BART  
620 model. *Statistics in Medicine* **38**, 5048–5069 (2019).
- 621 69. Bürkner, P.-C. Advanced Bayesian Multilevel Modeling with the R Package brms.  
622 *The R Journal* **10**, 395–411 (2018).
- 623 70. Modern Analytic Apps for the Enterprise. *Plotly* <https://plot.ly>.
- 624 71. Therneau, T. M., until 2009), T. L. (original S.->R port and R. maintainer, Elizabeth,  
625 A. & Cynthia, C. survival: Survival Analysis. (2023).
- 626 72. Thompson, C. G., Kim, R. S., Aloe, A. M. & Becker, B. J. Extracting the variance  
627 inflation factor and other multicollinearity diagnostics from typical regression  
628 results. *Basic and Applied Social Psychology* **39**, 81–90 (2017).
- 629 73. Ranstam, J. & Cook, J. A. LASSO regression. *British Journal of Surgery* **105**, 1348  
630 (2018).
- 631 74. Kassambara, A., Kosinski, M., Biecek, P. & Fabian, S. survminer: Drawing Survival  
632 Curves using ‘ggplot2’. (2021).
- 633 75. Löning, M. *et al.* sktime: A Unified Interface for Machine Learning with Time  
634 Series. Preprint at <https://doi.org/10.48550/arXiv.1909.07872> (2019).
- 635 76. Kalinowski, T. *et al.* reticulate: Interface to ‘Python’. (2023).
- 636 77. Lenth, R. V. *et al.* emmeans: Estimated Marginal Means, aka Least-Squares Means.  
637 (2023).
- 638 78. Ravvaz, K., Weissert, J. A. & Downs, T. M. American Urological Association  
639 Nonmuscle Invasive Bladder Cancer Risk Model Validation—Should Patient Age  
640 be Added to the Risk Model? *The Journal of Urology* (2019)  
641 doi:10.1097/JU.0000000000000389.

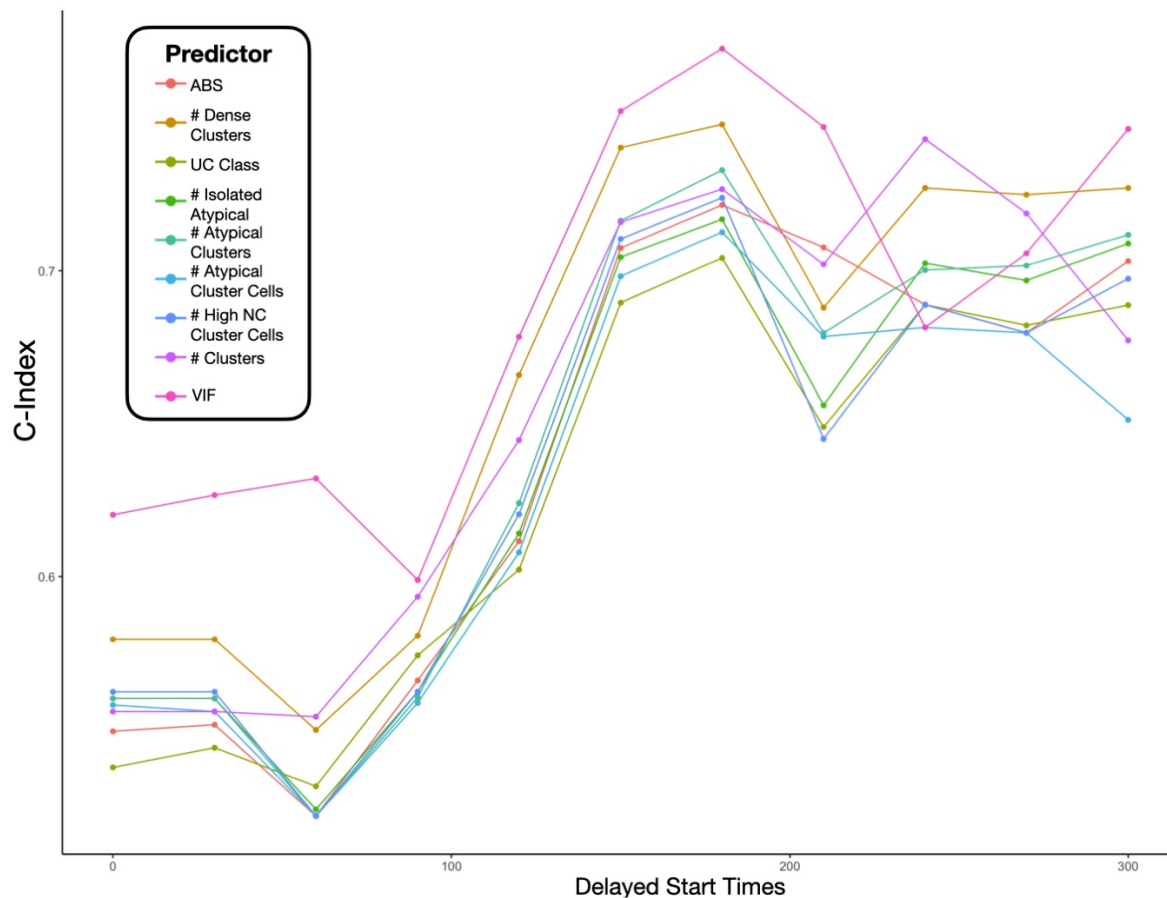


- 642 79. Vuong, Q. H. Likelihood ratio tests for model selection and non-nested hypotheses.  
643 *Econometrica* **57**, 307–333 (1989).
- 644 80. Chow, N.-H., Tzai, T.-S., Cheng, H.-L., Chan, S.-H. & Lin, J. S.-N. Urinary  
645 Cytodiagnosis: Can It Have a Different Prognostic Implication than a Diagnostic  
646 Test? *UIN* **53**, 18–23 (1994).
- 647 81. Liu, W. *et al.* Preoperative positive voided urine cytology predicts poor clinical  
648 outcomes in patients with upper tract urothelial carcinoma undergoing  
649 nephroureterectomy. *BMC Cancer* **20**, 1113 (2020).
- 650 82. Fan, B. *et al.* Predictive Value of Preoperative Positive Urine Cytology for  
651 Development of Bladder Cancer After Nephroureterectomy in Patients With Upper  
652 Urinary Tract Urothelial Carcinoma: A Prognostic Nomogram Based on a  
653 Retrospective Multicenter Cohort Study and Systematic Meta-Analysis. *Front Oncol*  
654 **11**, 731318 (2021).
- 655 83. Tokuyama, N. *et al.* Prediction of non-muscle invasive bladder cancer recurrence  
656 using machine learning of quantitative nuclear features. *Mod Pathol* **35**, 533–538  
657 (2022).
- 658 84. Li, R. C., Asch, S. M. & Shah, N. H. Developing a delivery science for artificial  
659 intelligence in healthcare. *npj Digit. Med.* **3**, 1–3 (2020).
- 660 85. Yildirim, N., Zimmerman, J. & Preum, S. Technical Feasibility, Financial Viability,  
661 and Clinician Acceptance: On the Many Challenges to AI in Clinical Practice. in  
662 *HUMAN@ AAAI Fall Symposium* (2021).
- 663 86. Salto-Tellez, M. More than a decade of molecular diagnostic cytopathology leading  
664 diagnostic and therapeutic decision-making. *Archives of pathology & laboratory*  
665 *medicine* **142**, 443–445 (2018).
- 666 87. Cai, C. J., Winter, S., Steiner, D., Wilcox, L. & Terry, M. ‘Hello AI’: uncovering the  
667 onboarding needs of medical practitioners for human-AI collaborative decision-  
668 making. *Proceedings of the ACM on Human-computer Interaction* **3**, 1–24 (2019).
- 669 88. Van Es, S. L., Kumar, R. K., Pryor, W. M., Salisbury, E. L. & Velan, G. M.  
670 Cytopathology whole slide images and adaptive tutorials for senior medical  
671 students: a randomized crossover trial. *Diagnostic Pathology* **11**, 1–9 (2016).
- 672 89. Yoder, B. J. *et al.* Reflex UroVysion Testing of Bladder Cancer Surveillance Patients  
673 With Equivocal or Negative Urine Cytology: A Prospective Study With Focus on  
674 the Natural History of Anticipatory Positive Findings. *American Journal of Clinical*  
675 *Pathology* **127**, 295–301 (2007).
- 676 90. Fine, J. P. & Gray, R. J. A Proportional Hazards Model for the Subdistribution of a  
677 Competing Risk. *Journal of the American Statistical Association* **94**, 496–509 (1999).
- 678 91. Austin, P. C., Putter, H., Lee, D. S. & Steyerberg, E. W. Estimation of the Absolute  
679 Risk of Cardiovascular Disease and Other Events: Issues With the Use of Multiple  
680 Fine-Gray Subdistribution Hazard Models. *Circulation: Cardiovascular Quality and*  
681 *Outcomes* **15**, e008368 (2022).
- 682 92. Barnwal, A., Cho, H. & Hocking, T. Survival Regression with Accelerated Failure  
683 Time Model in XGBoost. *Journal of Computational and Graphical Statistics* **31**, 1292–  
684 1302 (2022).
- 685 93. Sonabend, R., Király, F. J., Bender, A., Bischl, B. & Lang, M. mlr3proba: an R  
686 package for machine learning in survival analysis. *Bioinformatics* **37**, 2789–2791  
687 (2021).
- 688 94. Wang, Z. & Sun, J. Survtrace: Transformers for survival analysis with competing  
689 events. in *Proceedings of the 13th ACM International Conference on Bioinformatics,*  
690 *Computational Biology and Health Informatics* 1–9 (2022).

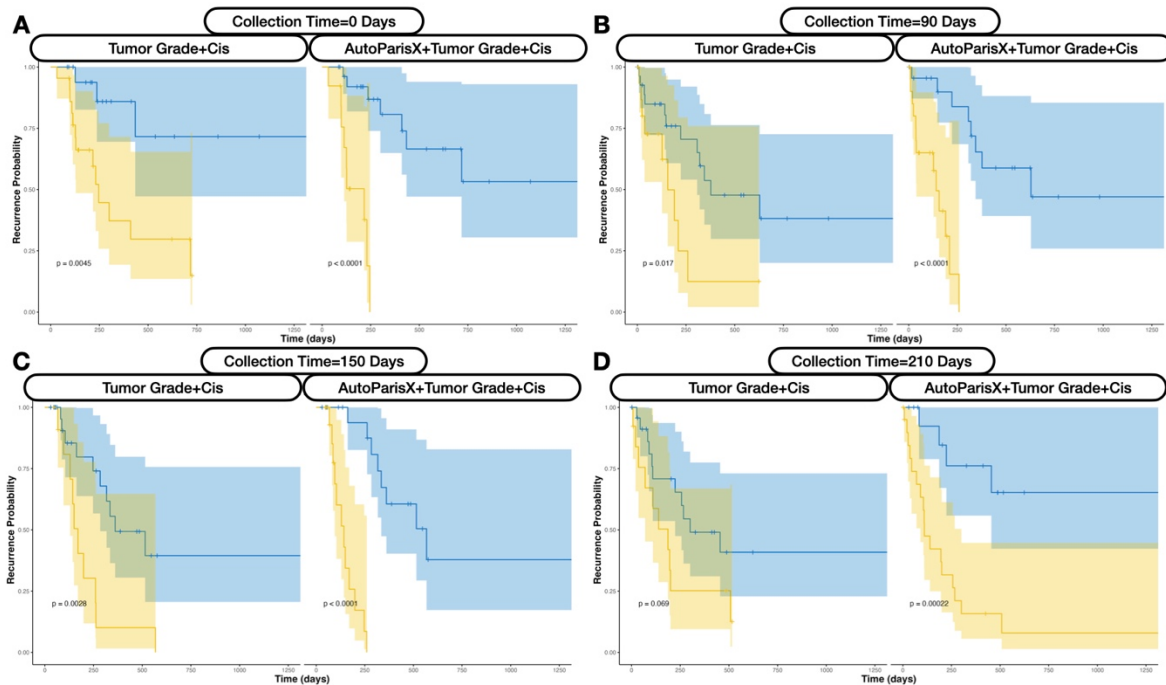
- 691 95. Kvamme, H., Borgan, Ø. & Scheel, I. Time-to-Event Prediction with Neural  
692 Networks and Cox Regression. *Journal of Machine Learning Research* **20**, 1–30 (2019).
- 693 96. Pölsterl, S. scikit-survival: A Library for Time-to-Event Analysis Built on Top of  
694 scikit-learn. *The Journal of Machine Learning Research* **21**, 8747–8752 (2020).
- 695 97. Davidson-Pilon, C. lifelines: survival analysis in Python. *Journal of Open Source*  
696 *Software* **4**, 1317 (2019).
- 697 98. Tang, W., Ma, J., Mei, Q. & Zhu, J. SODEN: A Scalable Continuous-Time Survival  
698 Model through Ordinary Differential Equation Networks. *J. Mach. Learn. Res.* **23**,  
699 34–1 (2022).
- 700 99. Nagpal, C., Potosnak, W. & Dubrawski, A. auton-survival: an Open-Source  
701 Package for Regression, Counterfactual Estimation, Evaluation and Phenotyping  
702 with Censored Time-to-Event Data. *arXiv preprint arXiv:2204.07276* (2022).
- 703 100. Scheike, T. H. & Zhang, M.-J. Analyzing competing risk data using the R timereg  
704 package. *Journal of statistical software* **38**, (2011).
- 705 101. Bender, A. & Scheipl, F. Pammtools: Piece-wise exponential additive mixed  
706 modeling tools. *arXiv preprint arXiv:1806.01042* (2018).
- 707 102. Wang, P., Li, Y. & Reddy, C. K. Machine learning for survival analysis: A survey.  
708 *ACM Computing Surveys (CSUR)* **51**, 1–36 (2019).
- 709 103. Alaa, A. M. & van der Schaar, M. Deep multi-task gaussian processes for survival  
710 analysis with competing risks. in *Proceedings of the 31st International Conference on*  
711 *Neural Information Processing Systems* 2326–2334 (2017).
- 712 104. Ranganath, R., Perotte, A., Elhadad, N. & Blei, D. Deep survival analysis. in  
713 *Machine Learning for Healthcare Conference* 101–114 (PMLR, 2016).
- 714 105. Fernández, T., Rivera, N. & Teh, Y. W. Gaussian processes for survival analysis.  
715 *Advances in Neural Information Processing Systems* **29**, (2016).
- 716 106. Levy, J. J. & O'Malley, A. J. Don't dismiss logistic regression: the case for sensible  
717 extraction of interactions in the era of machine learning. *BMC Med Res Methodol* **20**,  
718 171 (2020).
- 719 107. Birkenkamp-Demtröder, K. *et al.* Monitoring treatment response and metastatic  
720 relapse in advanced bladder cancer by liquid biopsy analysis. *European urology* **73**,  
721 535–540 (2018).
- 722 108. Crocetto, F. *et al.* Liquid biopsy in bladder cancer: State of the art and future  
723 perspectives. *Critical Reviews in Oncology/Hematology* 103577 (2022).
- 724 109. Ferro, M. *et al.* Liquid biopsy biomarkers in urine: A route towards molecular  
725 diagnosis and personalized medicine of bladder cancer. *Journal of personalized*  
726 *medicine* **11**, 237 (2021).
- 727 110. Lodewijk, I. *et al.* Liquid biopsy biomarkers in bladder cancer: a current need for  
728 patient diagnosis and monitoring. *International journal of molecular sciences* **19**, 2514  
729 (2018).
- 730 111. Huang, H.-M. & Li, H.-X. Tumor heterogeneity and the potential role of liquid  
731 biopsy in bladder cancer. *Cancer Communications* **41**, 91–108 (2021).
- 732 112. Oshi, M. *et al.* Urine as a source of liquid biopsy for cancer. *Cancers* **13**, 2652 (2021).
- 733 113. Todenhöfer, T., Struss, W. J., Seiler, R., Wyatt, A. W. & Black, P. C. Liquid biopsy-  
734 analysis of circulating tumor DNA (ctDNA) in bladder cancer. *Bladder Cancer* **4**, 19–  
735 29 (2018).
- 736 114. Wang, G. *et al.* Urine-based liquid biopsy in bladder cancer: Opportunities and  
737 challenges. *Clinical and Translational Discovery* **3**, e176 (2023).

- 738 115. Tsuneki, M., Abe, M. & Kanavati, F. Deep Learning-Based Screening of Urothelial  
739 Carcinoma in Whole Slide Images of Liquid-Based Cytology Urine Specimens.  
740 *Cancers* **15**, 226 (2023).
- 741 116. Nojima, S. *et al.* A deep learning system to diagnose the malignant potential of  
742 urothelial carcinoma cells in cytology specimens. *Cancer Cytopathology* **129**, 984–995  
743 (2021).
- 744 117. McAlpine, E. D. & Michelow, P. The cytopathologist’s role in developing and  
745 evaluating artificial intelligence in cytopathology practice. *Cytopathology* **31**, 385–  
746 392 (2020).
- 747 118. Karagas, M. R. *et al.* Design of an epidemiologic study of drinking water arsenic  
748 exposure and skin and bladder cancer risk in a US population. *Environmental health*  
749 *perspectives* **106**, 1047–1050 (1998).
- 750 119. Karagas, M. R., Stukel, T. A. & Tosteson, T. D. Assessment of cancer risk and  
751 environmental levels of arsenic in New Hampshire. *International journal of hygiene*  
752 *and environmental health* **205**, 85–94 (2002).
- 753 120. Nuckols, J. R. *et al.* Estimating water supply arsenic levels in the New England  
754 Bladder Cancer Study. *Environmental health perspectives* **119**, 1279–1285 (2011).
- 755 121. Koutros, S. *et al.* Potential effect modifiers of the arsenic–bladder cancer risk  
756 relationship. *International journal of cancer* **143**, 2640–2646 (2018).
- 757 122. Baris, D. *et al.* Elevated bladder cancer in Northern New England: the role of  
758 drinking water and arsenic. *JNCI: Journal of the National Cancer Institute* **108**, (2016).
- 759 123. Karagas, M. R. *et al.* Incidence of transitional cell carcinoma of the bladder and  
760 arsenic exposure in New Hampshire. *Cancer Causes & Control* **15**, 465–472 (2004).
- 761  
762  
763

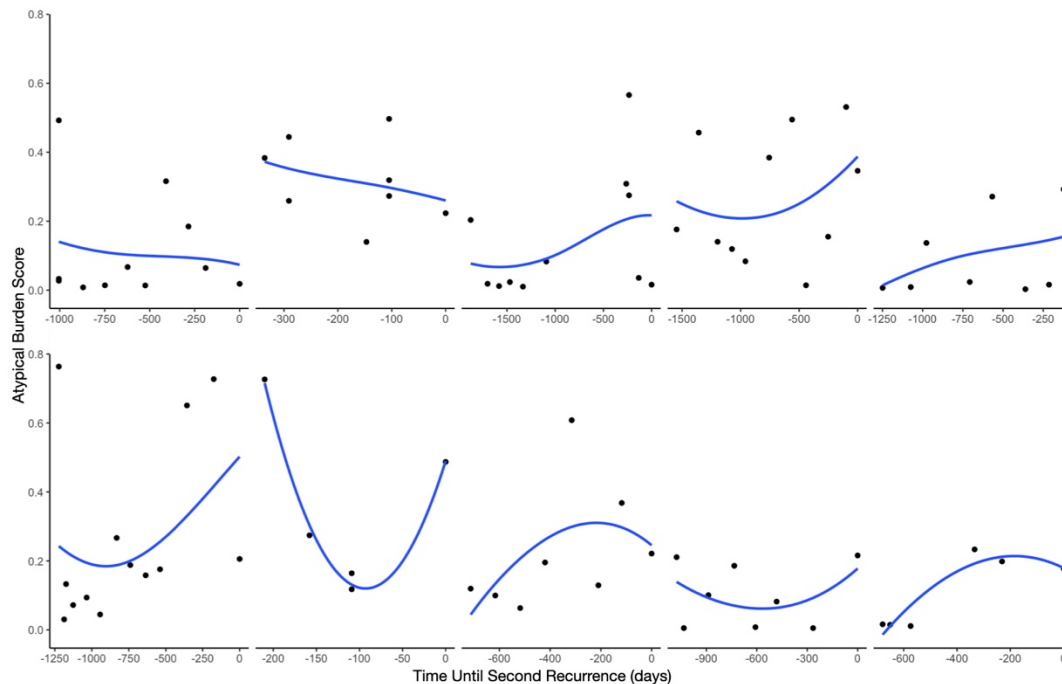
764 **Appendix**  
765



766 **Supplementary Figure 1: C-index for specific imaging / manual cytology exam results,**  
767 **reported based on different collection periods/times (days) prior to the recurrence risk follow-up**  
768 **period; only select AutoParis-X measurements of interest were reported**  
769  
770

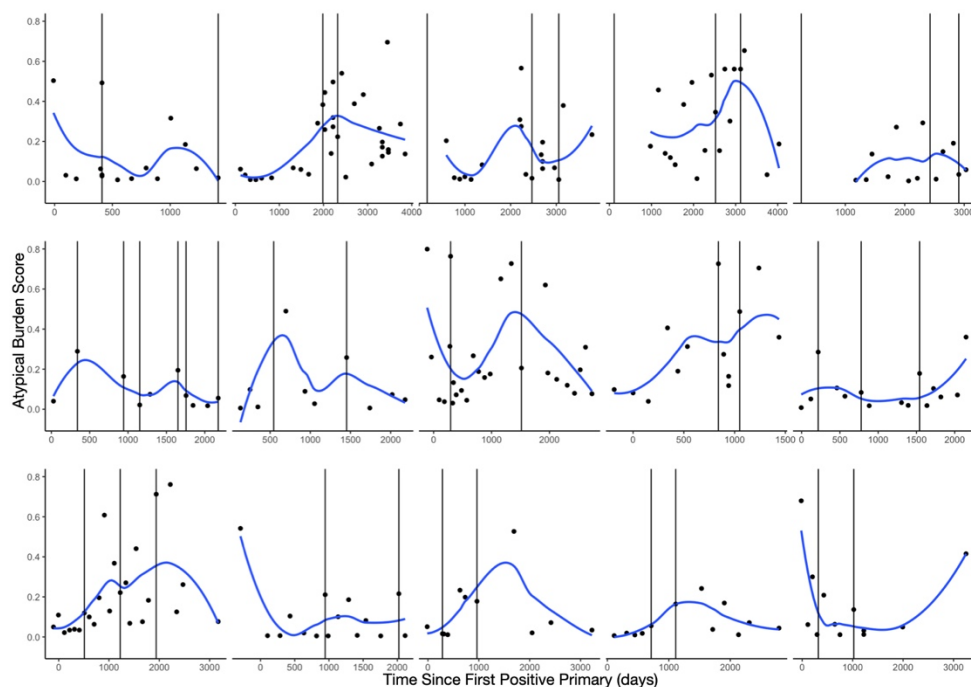


771  
772 **Supplementary Figure 2: Comparison of KM plots for Imaging versus Histological**  
773 **Predictors, for cytological information collected across the following collection time periods**  
774 **after the first positive primary: A) 0 days, B) 90 days, C) 150 days, D) 210 days**  
775



776  
777 **Supplementary Figure 3: Atypia Burden Score Versus Time Until Second Recurrence:**  
778 **Reported for 10 patients with at least 4 repeat exams across the period between their first and**  
779 **second recurrence**  
780

781



782

783

**Supplementary Figure 4: Atypia Burden Score Versus Time Across Multiple Recurrence Events for Select Patients:** Each recurrence date is represented with the vertical line

784

785

786

787

**Supplementary Table 1: Description of Slide Level predictors of Recurrence**

Level	Predictor	Algorithm	Description
Cell	Urothelial cell score	UroNet	Predicted probability of urothelial cell from convolutional neural network, used to dynamically isolate urothelial cells in specimen
	Atypia score	AtyNet	Predicted probability of presence of atypical features in urothelial cell (e.g., hyperchromasia, irregular nuclear membrane, etc.), determined using convolutional neural network
	NC Ratio	UroSeg	Nuclear to cytoplasm area ratio derived from pixelwise segmentation of nucleus and cytoplasm using segmentation neural network
	Morphometric measures	Custom	Complements binning of urothelial cells and assignment of atypia score, features: 1) area; 2) convex area; 3) eccentricity; 4) equivalent diameter; 5) extent; 6) Feret's diameter; 7) maximum diameter; 8) filled area; 9) major axis length; 10) minor axis length; 11) perimeter; and 12) solidity
Cluster	Dense Area	BorderDet	Whether cluster contains dense architecture of overlapping and indistinguishable cytoplasmic borders
	Number urothelial cells	BorderDet/UroNet	Whether cluster contained urothelial cells, determined by counting cells with high urothelial cell score
	Number atypical urothelial cells (atypia score)	BorderDet/UroNet/AtyNet	Whether cluster contained abnormal urothelial cells, determined by counting cells with high atypia score
	Number atypical urothelial cells (NC ratio)	BorderDet/UroNet/UroSeg	Whether cluster contained abnormal urothelial cells, determined by counting cells with high NC ratio
	Dense & Atypical	BorderDet/UroNet/AtyNet/UroSeg	Whether cluster contained both dense architecture and atypical cellular features

Slide	Patient characteristics	Supplied	Includes age, sex, history of hematuria, specimen source (e.g., voided), presence of specimen artifact
	Isolated Cell-SIF Scores	Bayesian Optimization	Counting the number of cells with the following features from cells not associated with clusters: 1) cellularity (urothelial score), 2) atypia (atypia score), 3) atypia (NC ratio), 4) other morphometric measures
	Cluster Cell-SIF Scores	Bayesian Optimization	Counting the number of cells with the following features from cells associated with clusters: 1) cellularity (urothelial score), 2) atypia (atypia score), 3) atypia (NC ratio), 4) other morphometric measures
	All Cell-SIF Scores	Bayesian Optimization	Combines Isolated Cell-SIF Scores and Cluster Cell-SIF Scores
	Cluster-SIF	Bayesian Optimization	Counting the number of clusters with the following features: 1) number of urothelial clusters, 2) atypical urothelial clusters (atypia score), 3) atypical clusters (NC ratio), 4) dense clusters, 5) dense and atypical clusters
	Atypia Burden Score	Mixed effects machine learning	Integrates all slide-level predictors using machine learning model to calculate a score between 0-1 reflecting overall specimen atypia, correlated with UC diagnostic category

788  
789  
790  
791  
792  
793  
794

**Supplemental Table 2:** Concordance statistics for *fixed predictors* at the following collection time periods; also included are performance statistics for *dynamic predictors* from the *time-varying covariate* cox model; the percentage of imaging variables which outperform manual examination is represented as “% Outperform UC Class”

Collection Time (days)	0		30		60		90		120		150	
Predictors	C	SE	C	SE	C	SE	C	SE	C	SE	C	SE
ABS	0.549	0.075	0.552	0.075	0.522	0.076	0.566	0.06	0.615	0.065	0.707	0.047
# Dense Clusters	0.62	0.069	0.62	0.069	0.6	0.069	0.581	0.061	0.666	0.066	0.74	0.051
UC Class	0.544	0.081	0.548	0.08	0.536	0.079	0.575	0.059	0.614	0.058	0.701	0.065
Eccentricity	0.558	0.084	0.564	0.088	0.515	0.078	0.557	0.059	0.662	0.059	0.716	0.048
# Isolated Atypical Cells	0.56	0.077	0.56	0.077	0.524	0.077	0.562	0.059	0.615	0.064	0.704	0.042
# Atypical Clusters	0.56	0.076	0.56	0.076	0.522	0.078	0.563	0.06	0.626	0.065	0.716	0.054
# Overall Atypical Cells	0.562	0.079	0.56	0.077	0.524	0.076	0.565	0.059	0.623	0.063	0.701	0.047
# Cluster Atypical Cells	0.558	0.076	0.556	0.075	0.522	0.076	0.561	0.059	0.623	0.062	0.698	0.047
% Clusters Dense/Atypical	0.554	0.076	0.554	0.076	0.519	0.077	0.564	0.06	0.631	0.051	0.683	0.054
# Isolated Cells High NC	0.558	0.081	0.558	0.081	0.522	0.076	0.564	0.058	0.617	0.063	0.713	0.047
# Overall Cells High NC	0.56	0.08	0.56	0.08	0.526	0.077	0.566	0.059	0.616	0.063	0.713	0.047
# Cluster Cells High NC	0.562	0.077	0.562	0.077	0.522	0.08	0.562	0.059	0.62	0.062	0.71	0.046
LASSO	0.59	0.084	0.603	0.073	0.578	0.069	0.584	0.06	0.654	0.058	0.74	0.051
# Cells	0.558	0.08	0.558	0.08	0.524	0.078	0.573	0.065	0.628	0.065	0.71	0.048
# Clusters	0.567	0.073	0.571	0.072	0.582	0.07	0.593	0.061	0.645	0.067	0.716	0.05
Overall	0.672	0.073	0.725	0.055	0.714	0.056	0.707	0.061	0.81	0.074	0.824	0.045
VIF	0.62	0.073	0.627	0.071	0.632	0.066	0.614	0.055	0.7	0.051	0.752	0.058
% Outperform UC Class	1.000	0.000	1.000	0.000	0.278	0.106	0.278	0.106	1.000	0.000	0.889	0.074

Collection Time (days)	180		210		240		270		300		Time Varying Covariates	
Predictors	C	SE	C	SE	C	SE	C	SE	C	SE	C	SE
ABS	0.722	0.048	0.708	0.051	0.689	0.063	0.68	0.067	0.703	0.06	0.652	0.039
# Dense Clusters	0.748	0.05	0.688	0.058	0.727	0.057	0.725	0.055	0.727	0.066	0.603	0.038
UC Class	0.724	0.062	0.673	0.063	0.689	0.06	0.682	0.059	0.689	0.059	0.579	0.05
Eccentricity	0.724	0.048	0.697	0.059	0.665	0.073	0.639	0.076	0.699	0.068	0.607	0.034

# Isolated Atypical Cells	0.717	0.043	0.692	0.056	0.702	0.065	0.697	0.066	0.709	0.061	0.612	0.039
# Atypical Clusters	0.733	0.053	0.716	0.062	0.7	0.067	0.702	0.064	0.712	0.06	0.62	0.039
# Overall Atypical Cells	0.715	0.048	0.679	0.062	0.685	0.069	0.682	0.068	0.663	0.067	0.638	0.04
# Cluster Atypical Cells	0.713	0.048	0.681	0.064	0.685	0.069	0.68	0.069	0.651	0.068	0.637	0.042
% Clusters Dense/Atypical	0.701	0.055	0.695	0.066	0.641	0.069	0.649	0.072	0.669	0.071	0.588	0.041
# Isolated Cells High NC	0.724	0.046	0.664	0.061	0.709	0.066	0.69	0.066	0.689	0.063	0.588	0.039
# Overall Cells High NC	0.727	0.047	0.655	0.054	0.707	0.066	0.685	0.065	0.709	0.062	0.564	0.042
# Cluster Cells High NC	0.724	0.047	0.645	0.057	0.697	0.068	0.68	0.066	0.699	0.068	0.541	0.044
LASSO	0.734	0.056	0.723	0.054	0.707	0.061	0.691	0.051	0.726	0.064	0.657	0.038
# Cells	0.724	0.045	0.705	0.052	0.707	0.058	0.692	0.063	0.712	0.059	0.631	0.039
# Clusters	0.727	0.049	0.702	0.053	0.743	0.051	0.719	0.056	0.677	0.067	0.6	0.039
Overall	0.827	0.046	0.849	0.051	0.927	0.035	0.92	0.036	0.911	0.03	0.659	0.041
VIF	0.773	0.058	0.747	0.057	0.731	0.061	0.743	0.074	0.746	0.06	0.682	0.036
% Outperform UC Class	0.611	0.115	0.722	0.106	0.667	0.111	0.611	0.115	0.667	0.111	0.778	0.098

795  
796  
797  
798  
799  
800  
801

**Supplemental Table 3: Comparison between Cytological Imaging Predictors Versus Histology:** Hazard ratios, 95% confidence intervals and p-values, specifically after adjusting for tumor grade/type, reported for a variable constructed from the imaging predictors alone; also includes p-values from partial likelihood ratio test assessing whether imaging cytological exams improves on histological predictors; reports for *fixed predictors* collected across various collection time periods

Collection Time (days)	log(HR)	2.5% CI	97.5% CI	p-value	p-value- H1: Imaging>Grade+Cis	p-value- H1: Imaging+Grade+Cis>Grade+Cis
0	1.258	0.569	1.947	0.00035	0.220	0.048
30	1.199	0.533	1.865	0.00042	0.220	0.054
60	0.980	0.429	1.531	0.00049	0.060	0.042
90	0.982	0.319	1.646	0.00370	0.144	0.130
120	1.003	0.519	1.488	0.00005	0.115	0.102
150	1.019	0.538	1.499	0.00003	0.055	0.059
180	1.051	0.563	1.539	0.00002	0.060	0.060
210	1.081	0.542	1.621	0.00009	0.026	0.028
240	0.962	0.455	1.470	0.00020	0.024	0.017
270	0.974	0.517	1.432	0.00003	0.020	0.022
300	1.021	0.452	1.589	0.00044	0.016	0.017

802  
803  
804  
805

**Supplementary Table 4: C-indices for Imaging Predictors from Time-Varying Effects Models**

Predictor	C	SE
ABS	0.65	0.039
Age	0.614	0.046
# Dense Clusters	0.578	0.037
UC Class	0.616	0.047
Eccentricity	0.563	0.049
Sex	0.54	0.041



# Isolated Atypical Cells	0.554	0.042
# Atypical Clusters	0.572	0.041
# Overall Atypical Cells	0.599	0.043
% Clusters Dense/Atypical	0.568	0.043
# Isolated Cells High NC	0.558	0.039
# Overall Cells High NC	0.557	0.04
# Cells	0.603	0.044
# Clusters	0.627	0.042
Overall	0.728	0.043

806  
807  
808  
809  
810

**Supplementary Table 5: Hazard Ratios for Imaging Predictors from Time Varying Effects Models;** Predictor effect size and significance is reported for every half year, which was used as the time periods to assess recurrence risk

Predictor	Time	log(HR)	2.5% CI	97.5% CI	z	Pr(> z )
# Overall Atypical Cells	0-180	1.39E-04	8.58E-05	1.93E-04	1.77E+00	7.63E-02
	180-360	3.08E-04	1.90E-04	4.26E-04	1.51E+00	1.32E-01
	360-540	4.60E-04	3.12E-04	6.07E-04	1.50E+00	1.33E-01
	540-720	7.25E-04	1.53E-04	1.30E-03	6.43E-01	5.20E-01
	720-900	-6.14E-04	-1.84E-03	6.08E-04	-6.91E-01	4.89E-01
	>900	1.38E-03	8.03E-04	1.95E-03	1.10E+00	2.69E-01
# Overall Cells High NC	0-180	2.03E-04	-2.87E-05	4.35E-04	6.93E-01	4.89E-01
	180-360	8.75E-04	4.99E-04	1.25E-03	2.35E+00	1.89E-02
	360-540	1.52E-03	9.92E-04	2.05E-03	1.29E+00	1.98E-01
	540-720	1.09E-03	-1.20E-04	2.30E-03	5.60E-01	5.75E-01
	720-900	-5.97E-05	-2.13E-03	2.01E-03	-3.43E-02	9.73E-01
	>900	8.15E-03	6.09E-03	1.02E-02	3.97E+00	7.23E-05
# Cells	0-180	4.72E-05	3.32E-05	6.11E-05	1.73E+00	8.39E-02
	180-360	5.16E-05	3.65E-05	6.66E-05	1.65E+00	9.90E-02
	360-540	-4.94E-06	-3.29E-05	2.31E-05	-1.32E-01	8.95E-01
	540-720	7.06E-05	4.95E-05	9.17E-05	2.49E+00	1.28E-02
	720-900	-1.07E-04	-2.38E-04	2.33E-05	-1.41E+00	1.58E-01
	>900	2.03E-04	1.43E-04	2.63E-04	1.58E+00	1.14E-01
Eccentricity	0-180	4.30E+00	1.89E+00	6.70E+00	8.73E-01	3.83E-01
	180-360	-1.60E+00	-3.89E+00	6.87E-01	-5.49E-01	5.83E-01
	360-540	3.97E+00	4.59E-01	7.47E+00	4.50E-01	6.53E-01
	540-720	1.72E+01	1.12E+01	2.31E+01	1.15E+00	2.49E-01
	720-900	6.20E+00	-2.94E+00	1.53E+01	3.73E-01	7.09E-01
	>900	5.72E+00	-1.11E+00	1.25E+01	4.22E-01	6.73E-01
# Isolated Atypical Cells	0-180	1.21E-04	-1.75E-04	4.17E-04	3.89E-01	6.98E-01
	180-360	4.85E-04	1.04E-04	8.67E-04	8.19E-01	4.13E-01
	360-540	2.02E-03	1.60E-03	2.44E-03	3.47E+00	5.22E-04
	540-720	1.15E-04	-2.23E-03	2.46E-03	2.37E-02	9.81E-01
	720-900	-4.80E-03	-9.49E-03	-1.21E-04	-7.92E-01	4.29E-01
	>900	2.19E-03	1.24E-04	4.25E-03	5.51E-01	5.82E-01
# Isolated Cells High NC	0-180	3.20E-04	-3.19E-04	9.60E-04	3.78E-01	7.05E-01
	180-360	2.70E-03	1.86E-03	3.54E-03	3.79E+00	1.51E-04
	360-540	2.33E-03	1.48E-03	3.18E-03	1.19E+00	2.34E-01
	540-720	4.15E-03	2.00E-03	6.30E-03	1.24E+00	2.13E-01
	720-900	-2.49E-03	-7.73E-03	2.75E-03	-6.05E-01	5.45E-01
	>900	1.43E-02	1.09E-02	1.77E-02	2.95E+00	3.15E-03
# Dense Clusters	0-180	2.85E-04	-5.81E-04	1.15E-03	2.38E-01	8.12E-01
	180-360	2.08E-03	1.54E-03	2.61E-03	4.87E+00	1.12E-06
	360-540	9.12E-03	7.59E-03	1.06E-02	4.20E+00	2.64E-05
	540-720	-1.02E-02	-1.91E-02	-1.20E-03	-9.38E-01	3.48E-01
	720-900	-4.12E-03	-1.39E-02	5.63E-03	-3.27E-01	7.44E-01
	>900	-3.12E-03	-1.12E-02	4.96E-03	-2.68E-01	7.89E-01

<b># Clusters</b>	0-180	8.60E-05	5.55E-05	1.16E-04	1.56E+00	1.20E-01
	180-360	1.39E-04	1.10E-04	1.69E-04	3.66E+00	2.50E-04
	360-540	4.19E-05	-9.12E-06	9.29E-05	4.55E-01	6.49E-01
	540-720	4.93E-05	-1.16E-05	1.10E-04	4.64E-01	6.43E-01
	720-900	-5.40E-04	-8.79E-04	-2.02E-04	-1.85E+00	6.48E-02
	>900	5.93E-05	-2.11E-05	1.40E-04	3.87E-01	6.99E-01
<b>% Clusters Dense/Atypical</b>	0-180	8.25E+00	5.08E+00	1.14E+01	1.93E+00	5.30E-02
	180-360	5.06E+00	-2.06E+00	1.22E+01	3.65E-01	7.15E-01
	360-540	2.56E+01	1.99E+01	3.14E+01	2.64E+00	8.39E-03
	540-720	-2.20E+01	-4.32E+01	-7.23E-01	-6.85E-01	4.93E-01
	720-900	3.74E+01	2.15E+01	5.34E+01	1.67E+00	9.44E-02
	>900	2.29E+01	7.72E+00	3.81E+01	1.02E+00	3.07E-01
<b># Atypical Clusters</b>	0-180	7.07E-04	2.25E-04	1.19E-03	1.39E+00	1.65E-01
	180-360	2.89E-03	1.76E-03	4.02E-03	1.53E+00	1.26E-01
	360-540	3.58E-03	2.71E-03	4.45E-03	2.12E+00	3.40E-02
	540-720	3.22E-03	-5.21E-04	6.96E-03	3.99E-01	6.90E-01
	720-900	-6.12E-03	-1.40E-02	1.74E-03	-5.87E-01	5.57E-01
	>900	4.81E-03	9.55E-04	8.67E-03	6.08E-01	5.43E-01
<b>ABS</b>	0-180	2.74E+00	2.17E+00	3.31E+00	3.00E+00	2.69E-03
	180-360	2.22E+00	1.57E+00	2.86E+00	1.72E+00	8.51E-02
	360-540	-1.86E-01	-1.22E+00	8.45E-01	-1.30E-01	8.96E-01
	540-720	8.28E-01	-5.97E-01	2.25E+00	2.75E-01	7.84E-01
	720-900	2.39E+00	6.42E-01	4.15E+00	9.43E-01	3.46E-01
	>900	7.96E+00	6.45E+00	9.47E+00	3.31E+00	9.41E-04
<b>UC Class</b>	0-180	1.61E+00	1.35E+00	1.88E+00	3.10E+00	1.96E-03
	180-360	8.31E-01	5.37E-01	1.13E+00	1.38E+00	1.68E-01
	360-540	-2.07E-01	-7.32E-01	3.19E-01	-2.03E-01	8.39E-01
	540-720	4.70E-01	-7.19E-02	1.01E+00	4.38E-01	6.61E-01
	720-900	1.29E+00	6.80E-01	1.91E+00	1.39E+00	1.64E-01
	>900	1.49E+00	1.00E+00	1.98E+00	1.55E+00	1.21E-01

811  
 812 **Supplementary Table 6: Results from beta regression models comparing recurrence risk to**  
 813 **ABS scores during distinct time periods; Coefficients B represents differences in ABS scores**  
 814 **between low and high risk patients at specific time periods; the final coefficient represents how**  
 815 **ABS scores are changing over time between the first and second recurrences**  
 816

Comparison	Time Period	B	2.5% CI	97.5% CI	p-value
<b>High vs low risk, days since positive primary</b>	<b>0-113</b>	-0.297	-1.169	0.575	0.506
	<b>114-204</b>	0.134	-1.212	1.479	0.846
	<b>205-295</b>	-0.806	-1.849	0.238	0.133
	<b>295-412</b>	-1.038	-1.888	-0.187	0.019
	<b>413-690</b>	-1.186	-1.957	-0.416	0.003
<b>High vs low risk, days until first recurrence</b>	<b>&gt;752</b>	-0.070	-0.645	0.505	0.812
	<b>752-391</b>	0.122	-0.438	0.683	0.669
	<b>390-227</b>	-0.496	-1.086	0.095	0.102
	<b>226-114</b>	0.093	-0.459	0.645	0.742
	<b>113-0</b>	-0.595	-1.193	0.003	0.053
<b>Days until second recurrence, starting from first recurrence</b>	<b>Time in days (continuous)</b>	0.001	0.000	0.001	0.018

817  
 818